Inverse velocity statistics in two-dimensional turbulence

Luca Biferale
Dipartimento di Fisica, Università di Roma "Tor Vergata," Roma, Italy
and INFM, Unità di Tor Vergata, Via della Ricerca Scientifica 1, I-00133 Roma, Italy

Massimo Cencini
Dipartimento di Fisica, Università di Roma "La Sapienza," Roma, Italy
and CNRS, Observatoire de la Côte d'Azur, B.P. 4229, F-06304 Nice cedex 4, France

Alesandra S. Lanotte[a)]
CNR, ISAC—Sezione di Lecce, Str. Prov. Lecce-Monteroni Km 1.200, I-73100 Lecce, Italy
and INFM, Unità di Tor Vergata, I-00133 Roma, Italy

Davide Vergni
Dipartimento di Fisica, Università di Roma "La Sapienza," Roma, Italy
and INFN, Unità di Ricerca di Roma "La Sapienza," P.le Aldo Moro 2, I-00185 Roma, Italy

(Received 8 May 2002; accepted 11 January 2003; published 4 March 2003)

We present a numerical study of two-dimensional turbulent flows in the enstropy cascade regime, with different large-scale energy sinks. In particular, we study the statistics of more-than-differentiable velocity fluctuations by means of two sets of statistical estimators, namely *inverse statistics* and *second-order differences*. In this way, we are able to probe statistical fluctuations that are not captured by the usual spectral analysis. We show that a new set of exponents associated to more-than-differentiable fluctuations of the velocity field exists. We also present a numerical investigation of the temporal properties of **u** measured in different spatial locations. © *2003 American Institute of Physics.* [DOI: 10.1063/1.1557527]

I. INTRODUCTION

Many natural phenomena display complex fluctuations over a wide range of spatial and temporal scales. Complexity usually manifests in the non-Gaussian properties of probability distribution functions (PDF). When PDFs at different scales do not collapse by a simple rescaling procedure one speaks about intermittency.[1] Such nontrivial rescaling properties may be exhibited by PDF tails or peaks, or both.[2] When intermittency manifests in the PDF tails, it means that regions of very intense bursting activity are present. This is typical of three-dimensional turbulent flows, where the velocity field is strongly intermittent and rough.[1]

However, there are examples of other important natural phenomena that develop simple PDF tails but nontrivial PDF cores. PDF peaks are associated to laminar fluctuations, i.e., "smooth" variations of the field. A physically relevant example is offered by two-dimensional turbulent flows, where the presence of long living coherent structures, e.g., vortices, is very well known (see Fig. 1). Two-dimensional (2-D) turbulence is characterized by two different transport processes: an inverse energy cascade from the forcing scale to larger scales and a direct enstrophy cascade from the forcing scale to smaller scales.[3,4] The inverse energy cascade shows a non-intermittent Kolmogorov 1941 scaling for the velocity field.[5–7] On the contrary, in the direct cascade, nontrivial vorticity fluctuations have been observed in dependence on the large-scale characteristics of the flow.[8–13] In this regime, the velocity field is differentiable, therefore the standard analysis (customarily applied in 3-D turbulence), based on moments of velocity increments (the so-called structure functions) is poorly informative. Indeed structure functions are dominated by the differential component of the signal:

$$S_p(r) = \langle [s(x+r) - s(x)]^p \rangle \sim r^p, \tag{1}$$

where with s we indicate either the u_x or the u_y velocity fields component. It is worth stressing that the scaling behavior (1) does not imply that the velocity statistics is trivial. For example, it is well known that in the enstrophy cascade regime the energy spectrum shows a power law $E(k) \propto k^{-\alpha}$ with $\alpha \geqslant 3$, which is the signature of significant more-than-differentiable velocity fluctuations. Hence, subdominant contributions to the $s(x+r) - s(x) \propto r$ behavior must be present and, in principle, detectable. The triviality of the scaling (1) is just the consequence of not having chosen the suitable observable. Therefore, to extract interesting information on the statistics of smooth signals, new statistical tools are needed.

Recent contributions have shown that laminar events are optimally characterized in terms of their exit-distance statistics, also known as *inverse statistics*.[14–18] In a nutshell, in such approach one "inverts" the usual way of looking at signals. Standard analysis studies the statistics of signal increments over a certain spatial (or temporal) interval; the exit-distance approach looks at the statistics of spatial (temporal) intervals necessary to observe a given signal incre-

a)Author to whom correspondence should be addressed. Telephone: +39 0832 320720; fax: +39 0832 320716; electronic mail: a.lanotte@isac.cnr.it

 © 2003 American Institute of Physics

Downloaded 01 Oct 2011 to 130.89.86.11. Redistribution subject to AIP license or copyright; see http://pof.aip.org/about/rights_and_permissions

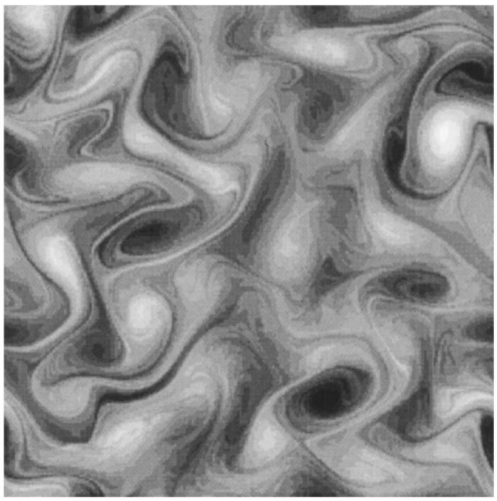

FIG. 1. A snapshot of the vorticity field. B/W intensity is coded according to the value of the vorticity field from the minima of ω (black) to the maximum (white). DNS have been performed by a standard dealiased pseudospectral algorithm, over a double periodic square domain of size $L=2\pi$, at resolution 512^2, 1024^2, and 2048^2. As customary, enstrophy is dissipated at small scales with a hyperdissipation of order 4, while energy is removed at large scales, to avoid piling up on the smallest mode, using different drags (see Table I). As to the pumping, we considered a Gaussian, white-in-time large-scale forcing restricted on wave numbers, $4<k_f\leqslant 6$.

ment. Another possibility to study smooth signals is to eliminate the differentiable contribution by looking at *second-order differences* (SD), i.e., $(s(x+r)-2s(x)+s(x-r))$ as suggested in Ref. 19.

In this paper we considerably extend a previous preliminary investigation[18] of the inverse statistics of velocity fields in the enstrophy cascade regime of 2-D turbulence, and also explore second-order difference statistics on the same flows. We present both exact analytical results for the exit-distance probability density functions of a 1-D Gaussian signal, and a set of numerical investigations of spatial and temporal statistics of 2-D turbulent flows. The main result is the introduction of a set of exponents that characterizes smooth behaviors beyond the energy spectrum slope α [where $E(k)\propto k^{-\alpha}$], and point out the presence of nontrivial contributions to the more-than-differentiable velocity fluctuations.

As it is well known, 2-D turbulence in the enstrophy cascade regime is strongly nonuniversal, i.e., a change in the large-scale forcing and drag mechanism is reflected in a drastic change in the spectrum slope. Many cases have been found with spectra slopes going from the classical $\alpha=-3$ (plus logarithmic corrections) to $\alpha=-6$. Such a strong nonuniversal behavior has direct consequences on the small-scale vorticity statistics, from the extremely rough vorticity field predicted by the Kraichnan argument[3,4] to the smooth vorticity field in the case $\alpha=-6$. Moreover, up to now, it was not clear whether nonuniversality of two-dimensional turbulence could be satisfactorily summarized by the spectrum dependency or if there is something beyond it, i.e., if there are nontrivial intermittent fluctuations in the small-scale vorticity dynamics. In particular, the velocity field statistics has never been studied in great detail. In this paper, we show that both inverse statistics and second-order difference statistics are able to assess in a quantitative and independent way the presence of nontrivial *anomalous* small-scale leading (subleading) velocity (vorticity) fluctuations. Such findings have important consequences for our understanding of vortex dynamics and on the statistical behavior. Inverse statistics measures the *persistency* properties of velocity/vorticity values along a one-dimensional cut of the 2-D field. The presence of anomalous behavior in the inverse statistics moments have to be connected to the existence of a much higher probability to observe a strongly persistent velocity fluctuation than predicted by a simple dimensional argument, based on the spectrum behavior only. This fact is further highlighted by a comparison with the statistics of the same signal but with random velocity phases. In that case, see below, inverse statistics becomes trivial, i.e., no ''more persistent'' velocity/vorticity events are detected.

The paper is organized as follows. In Sec. II, we recall some known results on 2-D turbulent flows in the presence of a drag mechanism at large scales. In Sec. III, we introduce the main observable, i.e., the inverse structure functions and the second-order difference structure functions: we first analyze Gaussian stochastic signals with a given spectrum $E(k)\sim k^{-\alpha}$, where we are able to establish some exact results. Then in Sec. IV, we present the spatial statistics of laminar fluctuations of velocity field, **u**, obtained by direct numerical simulations (DNS) of two-dimensional turbulence. In Sec. V, we perform a temporal analysis of the velocity field on fixed spatial locations. Section VI is devoted to conclusive remarks.

II. TWO-DIMENSIONAL TURBULENCE

As far as the inertial range of scales for the enstrophy cascade of two-dimensional turbulence is concerned, previous experimental, theoretical, and numerical studies have shown that the statistics is strongly influenced by large-scale phenomena. Indeed, *more than smooth* spectra, i.e., $E(k)\sim k^{-\alpha}$ with $\alpha>3$, depending on the characteristics of the forcing and of the large-scale dissipation, have been reported.[8–11] Recently, new results have clarified the problem in the case of the large-scale energy sink given by a linear (Eckman) friction.[9,10,12] The presence of an energy sink at large scales is conceptually justified by the necessity of avoiding the pile-up of energy on the gravest mode as a result of the inverse energy cascade,[5] and it is physically motivated in terms of the friction to which a fluid is subjected in the Eckman layer.[20,21]

The strong influence of large-scale physics in the enstrophy cascade range is believed to be a consequence of nonlocal interactions (in Fourier space). Another property associated to the enstrophy cascade is the velocity field smoothness.

Let us now fix the notation. In terms of the scalar vorticity $\omega=\nabla\times\mathbf{u}$, the equation of motion can be written as

$$\partial_t\omega+\mathbf{u}\cdot\nabla\omega=(-1)^{+q}\nu_q\Delta^q\omega+(-1)^{1-\rho}\beta_\rho\Delta^{-\rho}\omega+F, \tag{2}$$

Downloaded 01 Oct 2011 to 130.89.86.11. Redistribution subject to AIP license or copyright; see http://pof.aip.org/about/rights_and_permissions

where ν_q and $\beta_\rho(q,\rho\geqslant 0)$ are the coefficients of the generalized dissipations, namely the hyperdissipative and the hypofriction terms, respectively. The former removes enstrophy at small scales, while the latter dissipates energy at large scales. In particular, we used a hyperdissipation of order $q=4$ and various choices for the hypofriction exponent ρ. We also made some tests by using standard dissipation $q[1]$ without detecting any important differences: these results are not shown and in the sequel we report only those for $q=4$. F is the vorticity source term acting at large scales. In Fig. 1, we show a typical snapshot of the vorticity field obtained by the direct numerical simulation of Eq. (2). As one can see the vorticity field is characterized by filamental structures over a wide range of scales.

According to the classical prediction,[3,4] the velocity field should exhibit a Batchelor–Kraichnan spectrum, $E(k)\sim k^{-3}(\ln(k))^{-1/3}$. The dimensional estimate has been observed in a bunch of numerical and experimental measurements.[22,23] However, there are numerous situations where different velocity spectra have been measured:[8–12] $E(k)\sim k^{-\alpha}$, with the exponent α larger than 3 and dependent on the large-scale forcing and friction. In the case of linear friction ($\rho=0$), it is known that vorticity statistics is intermittent. In such a case, it has been recently clarified[9,10,12] that, at scales small enough, vorticity behaves as a passive scalar.[12] In particular, this has led to a quantitative understanding of the friction effects on the spectrum slope. By assuming the smoothness of the small scales velocity field and using a simple mean field argument, it has been shown[9,10] that $\alpha=3+2\beta_0/\lambda$, where λ is the Lagrangian Lyapunov exponent and β_0 is the drag coefficient; in other words, by increasing the drag coefficient, the spectrum becomes steeper. Actually, in order to exactly compute the spectrum slope, one has to go beyond the simple mean field analysis and consider the distribution of a finite time Lyapunov exponent (for details, see Refs. 9, 10, and 12).

Except for the situation with a large-scale linear friction, there is no general theory for the scaling properties of 2D turbulent flows in the presence of different large-scale drag mechanisms (see Ref. 24 for a recent attempt in this direction).

III. INVERSE AND DIRECT STATISTICS FOR SMOOTH SIGNALS

Let us introduce the inverse statistics and the second-order difference structure functions. We start applying them to the analysis of stochastic one-dimensional signals with a given spectrum $E(k)\sim k^{-\alpha}$. In particular, we consider smooth random signals built as follows:

$$s(x)=\sum_k \hat{s}(k)e^{i(kx+\theta_k)}, \tag{3}$$

where $|\hat{s}(k)|^2\sim k^{-\alpha}$ and θ_k are random phases, uniformly distributed in $[0,2\pi)$. For the sake of simplicity, we limit our discussion to signals with $3\leqslant\alpha<5$ (i.e., to smooth signals but only one time differentiable), for which we are able to establish some exact results. Note that for such signals, moments of differences over any increment r always possess a differentiable scaling (1), while moments of order $p\leqslant -1$ do not exist.

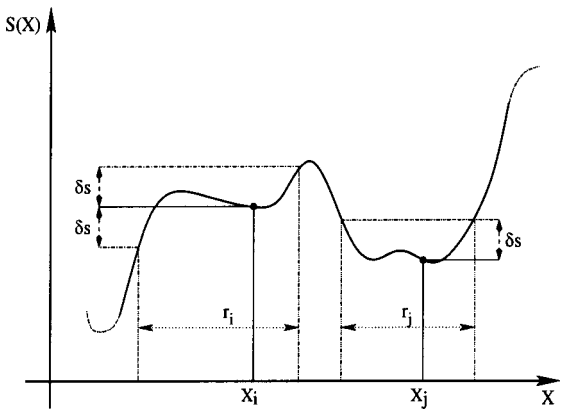

FIG. 2. Schematic representation of the exit-distance method. X_i and X_j are two points picked at random and r_i and r_j are the corresponding exit distances from the barrier δs.

A. Inverse statistics

For a generic one-dimensional signal $s(x)$, looking at inverse statistics consists in measuring moments of the distance, $r(\delta s)$, necessary to observe in the signal a double exit (forward and backward) through a barrier δs.

We fix a value for the signal fluctuations, δs, then we pick at random a point x_0 and measure the first forward $(|s(x_0+r_f)-s(x_0)|\geqslant\delta s)$ and backward $(|s(x_0-r_b)-s(x_0)|\geqslant\delta s)$ exit from the barrier, $r(\delta s)$. Then we put $r(x_0,\delta s)=r_b+r_f$. See Fig. 2 for a schematic view of the method. Repeating the observations for many points, $\{x_0\}$, and for different barrier heights, we can define the inverse structure functions[14] as

$$T^{(p)}(\delta s)=\langle r^p(\delta s)\rangle\sim\delta s^{\chi(p)}, \tag{4}$$

where the average is taken with respect to the random choice of the point x_0 (see the note in Ref. 25).

For the case of simple signals such as (3), the scaling exponents of inverse statistics moments can be derived as follows. If $3\leqslant\alpha<5$, the signal increment can be written as

$$s(x+r)-s(x)\sim\frac{ds(x)}{dx}r+c(x)r^h. \tag{5}$$

Here we have only kept the two most important scaling behaviors: $O(r)$ because of the differentiability and $O(r^h)$ from the spectrum exponent. The scaling exponent $1\leqslant h<2$ is related to the spectrum slope by the dimensional relation $\alpha=1+2h$, while $c(x)$ is a continuous function of x. By studying the exit event, in the limit of a small barrier height, we may observe two different kinds of events. The first, with probability one, is the differentiable scaling $r(\delta s)\sim\delta s$. The second, observed at those points where the first derivative vanishes, is the subleading behavior, $O(r^h)$, in (5)

One may estimate the probability of this second situation as follows. With $3\leqslant\alpha<5$ the first derivative is a self-affine signal with Hölder exponent $\xi=(h-1)<1$, which vanishes

Downloaded 01 Oct 2011 to 130.89.86.11. Redistribution subject to AIP license or copyright; see http://pof.aip.org/about/rights_and_permissions

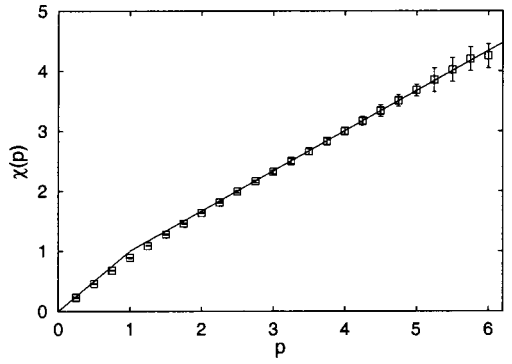

FIG. 3. Scaling exponents $\chi(p)$ of the inverse statistics for the 1-D signal (3) with $\alpha=4$. The solid line gives the bifractal behavior. Moments have been computed using 10^3 realizations of the signal (3) with 2^{17} modes; for each realization 2^{12} points have been taken at random.

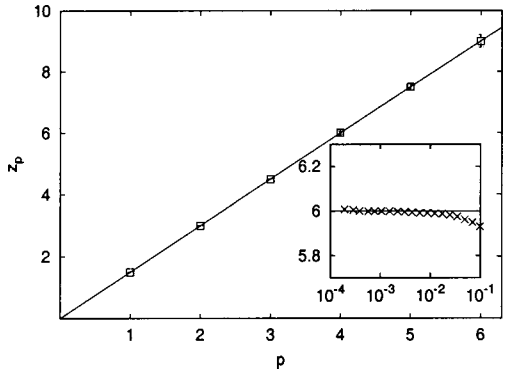

FIG. 4. Scaling exponent z_p of the SD statistics for the 1-D signal (3) with the same parameters as in Fig. 3, the straight line shows the expected behavior $z_p=hp$ with $h=1.5$. The inset shows the local slope for $p=4$.

on a fractal set of dimension $D=1-\xi=2-h$. Therefore, the probability to see the subleading term $O(r^h)$ dominating the exit event in (5) is given by the probability to pick at random a point on a fractal set of dimension D, i.e.,

$$P[r\sim(\delta s)^{1/h}]\sim r^{1-D}=(\delta s)^{1-1/h}. \tag{6}$$

Taking into account both events, we end with the following *bifractal* prediction for inverse statistics moments:

$$T^{(p)}(\delta s)\sim(\delta s)^{\chi_{\rm bf}(p)}, \quad \chi_{\rm bf}(p)=\min_h\left(p,\frac{p}{h}+1-\frac{1}{h}\right). \tag{7}$$

From (7), we conclude that laminar differentiable fluctuations influence the inverse statistics only up to moments of order $p=1$; for larger p, the PDF is dominated by the subdominant behavior, $[s(x+r)-s(x)]\sim r^h$. In other words, the extrema of the signal play the role of singularities for the inverse statistics: close to the extrema, events with much longer exit distances are observed when $\delta s\to 0$. For one-dimensional signals s (3) the prediction is verified with high accuracy (see Fig. 3).

In the general multiaffine case, signal increments scale as $\delta_r s(x)\sim r^{h(x)}$ with probability $P_r(h)\sim r^{1-D(h)}$, where the function $D(h)$ can be interpreted as the fractal dimension of the set where the Hölder exponent h is observed.[26]

For such a signal, it is possible to obtain[14,15] a link between the inverse statistics exponents, $\chi(p)$, and the fractal dimension, $D(h)$:

$$\chi(p)=\min_h\left(\frac{p+1-D(h)}{h}\right). \tag{8}$$

In the case of the smooth signal (3), one can see that (8) coincides with the bifractal prediction (7), as soon as we write $D(h)=2-h$ for $h\equiv\min[1,(\alpha-1)/2]$.

B. Second-order difference structure functions

Another way to eliminate the trivial differential scaling and extract some statistical information from smooth signals has been suggested in Ref. 19. The idea is to consider moments of the second-order difference $\Delta_r s\equiv[s(x+r)+s(x-r)-2s(x)]$, so as to eliminate the differentiable contribution $\delta_r s\propto r$. For the signals under investigation, we have that at the leading order $\Delta_r s\sim r^h$ with $1\leqslant h<2$, and moments behave as

$$S_{SD}^{(p)}(r)\equiv\langle|\Delta_r s|^p\rangle\sim r^{z_p}. \tag{9}$$

In the monofractal case (globally self-similar signals), one expects $z_p=ph$. The analysis done for the same stochastic 1-D signal of (3) with $h=1.5$, confirms this expectation (see Fig. 4).

In the general case, i.e., when many more-than-differentiable fluctuations are present, the scaling exponents z_p are nontrivially related to the distribution of the h exponents. The difficulty to give a multifractal prediction for $\Delta_r s$ increments stems from the fact that it is a three-point quantity, depending on the simultaneous fluctuations between $(x,x-r)$and $(x,x+r)$. Therefore, to draw the multifractal picture, we would need, in addition, a complete control of the spatial correlations. This is, in principle, feasible,[27,28] but it is left for future investigation.

IV. SPATIAL STATISTICS IN 2-D SMOOTH VELOCITY FIELDS

Let us now analyze the inverse and second-order difference statistics of the two-dimensional velocity field obtained by DNS of the Navier–Stokes equation (2). We performed four different sets of numerical experiments, with periodic boundary conditions on a spatial grid of 1024^2 collocation points. In all of them, we considered a Gaussian forcing, δ-correlated in time, with support in a restricted band of wave numbers $4<k_f\leqslant 6$.

In three out of four simulations, we used an Eckman linear friction, i.e., $\rho=0$ in (2) with different coefficients (simulations A,B,C, in the following). In the fourth run, we used a hypodiffusive term at large scales, $\rho=2$ (referred to as case D in what follows). Table I is a summary of the DNS parameters, together with the best-fit spectrum exponent α for all runs. In addition, to check the importance (if any) of finite Reynolds number effects in our results, we repeated one out of the four runs at the resolution of 2048^2 collocation points.

In Fig. 5 we show the averaged velocity spectrum for runs B, C, and D (run A gives a slope almost coincident with

Downloaded 01 Oct 2011 to 130.89.86.11. Redistribution subject to AIP license or copyright; see http://pof.aip.org/about/rights_and_permissions

TABLE I. Drag parameters ρ, β_ρ, spectrum slope α, and the real space subleading scaling exponent, $h=(\alpha-1)/2$ for the various numerical experiments. The value of each α has been obtained by a best fit in the region $|\mathbf{k}|\approx(20-100)$ (see Fig. 5). By performing the fit in the region $|\mathbf{k}|\approx(15-60)$, slightly larger values of α are obtained. These discrepancies can be associated to the interplay between the inverse cascade of energy and the friction acting on it, which contaminates the upper part of the spectrum.

DNS label	ρ	β_ρ	α	h
A	0	0.01	3.26(8)	1.14
B	0	0.10	3.4(1)	1.2
C	0	0.30	3.7(1)	1.35
D	2	14.0	3.26(8)	1.13

that of run D). By comparing them, it is evident that the spectrum slope depends on both the drag coefficient (runs A, B, and C) and on the drag mechanism (run D).

Evidently, we are in the presence of large-scales effects that somehow affect small-scale velocity fluctuations. We want now to quantify this statement by using the inverse statistics analysis. First, we compare the inverse structure functions measured on several snapshots of the DNS, with those obtained after randomization of all velocity phases on the same frames. The rationale for this test is to investigate the importance of correlations between fluctuations at different wave numbers and therefore the ''information'' content brought by coherent structures in 2-D turbulent flows.

If we look at a one-dimensional cut of the velocity field, before and after phases randomization, it is rather difficult to distinguish the original DNS field from that one with randomized phases. This is due to the steepness of the spectrum, i.e., only a few modes dominate the real-space configuration. Despite the apparent similarity, big differences arise when looking at inverse moments.

Because of the limited numerical resolution, the only quantitative statements one can give are for relative scaling properties. Therefore, we measure scaling laws of the inverse statistics by plotting all moments $T^{(p)}(\delta u)$ versus a reference one, say $T^{(2)}(\delta u)$. This is the same technique called ESS,[29] fruitfully applied in the analysis of 3-D turbulent data with

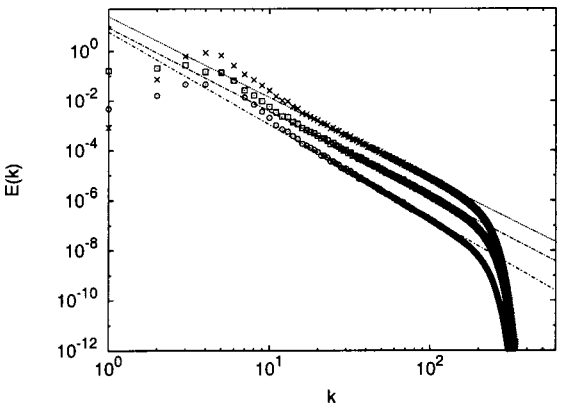

FIG. 5. A log–log of the energy spectra for two different drag coefficients with the Eckman linear friction, run B (middle) and run C (bottom), and with a hypofriction, run D (top). Straight lines correspond to the best fit power laws, $k^{-3.4}$, $k^{-3.7}$ and $k^{-3.26}$, respectively. Run A is not shown because it is almost indistinguishable from run D.

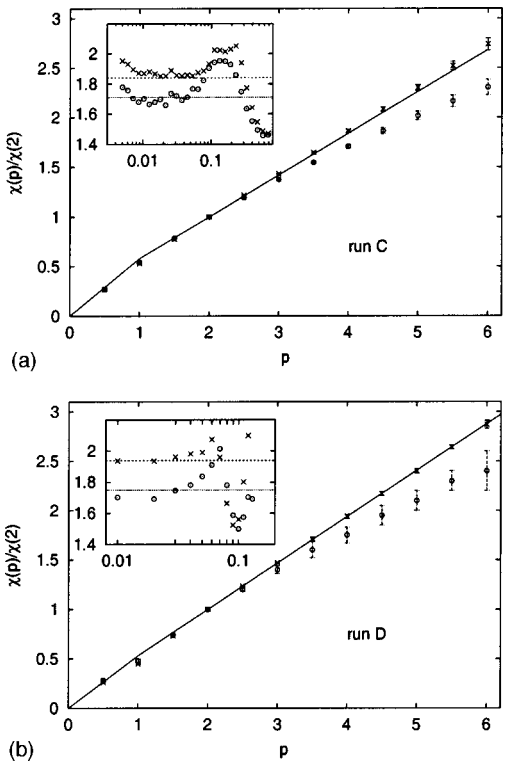

FIG. 6. $\chi(p)/\chi(2)$ for exit moments obtained in run C (a) and run D (b) (○), compared with the same data after phases randomization (×). In both figures, the solid line corresponds to the bifractal prediction. The value of h used for the theoretical prediction are obtained from the spectrum scaling exponents (see Table I), namely $h=1.35$ (run C) and $h=1.13$ (run D). Errors on scaling exponents have been computed according to the fluctuations of the local slopes. In each inset, it is shown the local slope of $T^{(4)}(\delta u)$ vs $T^{(2)}(\delta u)$ for the true signal (○) and the randomized one (×).

the aim of reabsorbing some finite-size effects and extracting scaling information also at moderate resolution. Therefore, we concentrated on the following relative scaling properties:

$$T^{(p)}(\delta u)\propto(T^{(2)}(\delta u))^{\chi(p)/\chi(2)}.$$

In Figs. 6(a) and 6(b) we summarize our findings. Inverse moment exponents, $\chi(p)/\chi(2)$, measured on the turbulent fields with randomized phases follow the bifractal prediction (7) with the value of h extracted from the spectrum (see Table I). Conversely, the longitudinal and transversal inverse statistics moments without phases randomization show anomalous scaling laws, which deviate from the bifractal law (7). In Figs. 6(a) and 6(b), we show the curve $\chi(p)/\chi(2)$ for both randomization and nonrandomized transversal exit moments for runs C and D. For $p<1$, the statistics of the randomized data and that of the turbulent data almost coincide being those moments (with $0<p<1$) dominated by the laminar fluctuations $u(x+r)-u(x)\sim r$. To better appreciate differences in the scaling curves, we show in the inset of Figs. 6(a) and 6(b) the local slopes of $T^{(4)}(\delta u)$ vs $T^{(2)}(\delta u)$, for the randomized and nonrandomized data.

The following scenario can be drawn. Inverse statistics of velocity increments in 2-D turbulent data is intermittent, i.e., the probability to observe at small scales a very smooth velocity realization is much higher than predicted by using a dimensional argument based on the spectrum only. This is

Downloaded 01 Oct 2011 to 130.89.86.11. Redistribution subject to AIP license or copyright; see http://pof.aip.org/about/rights_and_permissions

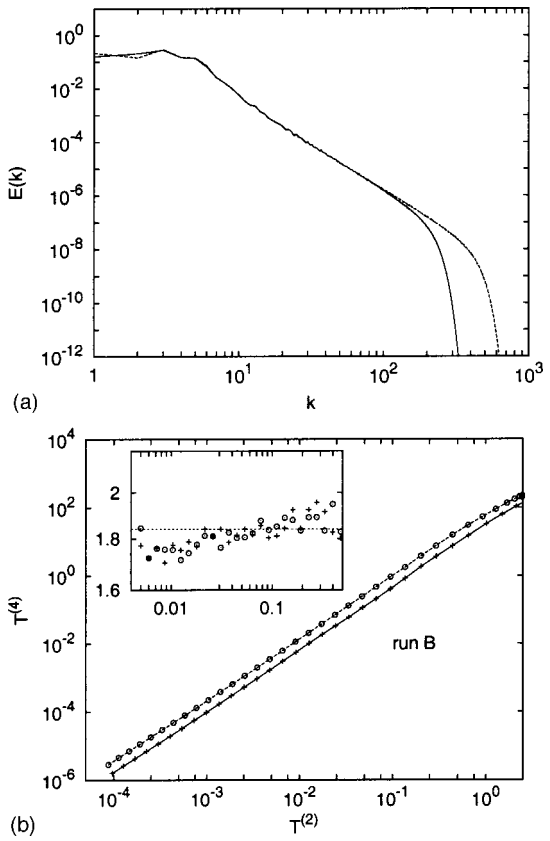

FIG. 7. (a) A log–log plot of the energy spectra for run B at the two resolutions 1024^2 and 2048^2. In (b), a log–log plot of the moment $T^{(4)}(\delta u)$ vs $T^{(2)}(\delta u)$ for the true signal: (○) at resolution 1024^2, (+) at resolution 2048^2 (the two curves have been shifted for plotting purposes). In the inset, the local slopes of the curves, the same symbols as before, i.e., (○) at resolution 1024^2, (+) at resolution 2048^2.

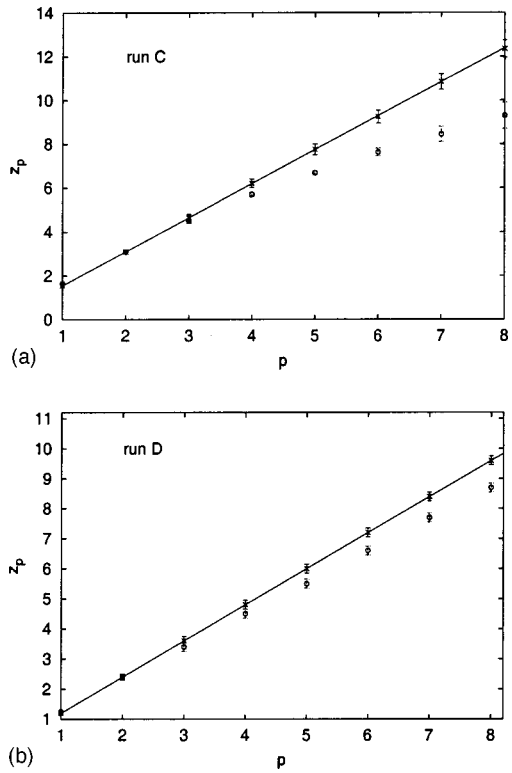

FIG. 8. (a) Second-order difference exponents, z_p, obtained in run (C) (○) and after randomization (×); (b) the same, but for run D. The straight lines correspond to the monofractal behavior $z_p = \tilde{h}p$ with $\tilde{h} = 1.55$ (run C) and $\tilde{h} = 1.20$ (run D).

connected to a nontrivial phase correlation of the small-scale velocity field, as proven by the return to the simple bifractal distribution after phase randomization. Concerning the degree of universality of smoother-than-differentiable fluctuations we observe, within error bars, the same degree of intermittency for the relative scaling exponents $\chi(p)/\chi(2)$ at changing the large-scale drag mechanism/coefficient. This cannot exclude some subtle dependency on the large-scale physics for higher moments.

Concerning the convergence of the results with Reynolds number, we repeated run B at resolution 2048^2.

In Fig. 7(a), a first check is done by comparing the energy spectra at the two numerical resolutions. In Fig. 7(b) we compare, for the turbulent signal, the ESS plots of the moment $T^{(4)}(\delta u)$ versus the reference one $T^{(2)}(\delta u)$, at the two resolutions. In the inset, the comparison of the local slopes confirms the quality of the numerical convergence of the results. Within the fluctuations of the local scaling exponents, simulations at 2048^2 collocation points fully reproduce the results of the run at 1024^2, giving a strong indication that at the working resolution there are no important Reynolds effects.

For the second-order difference statistics, analogous results have been found, that is a monofractal behavior for the randomization field and an anomalous behavior for the turbulent one. In Figs. 8(a) and 8(b), we show the scaling exponents z_p for run C and run D. Longitudinal and transversal components, within the errors coincide. The SD analysis confirms that the statistics of laminar events for the 2-D turbulent velocity field displays a multifractal structure.

Concerning the case of runs with linear friction, it is interesting to compare the results of the second-order difference moments with some recent analytical results.[30] In Ref. 30, it is argued that in the presence of linear Eckman friction, the second- and third-order (standard) structure functions behave as $S_2(r) = \langle \delta u^2(r) \rangle \sim ar^2 + br^{2+(\alpha-3)}$ and $S_3(r) = \langle (\delta u(r))^3 \rangle \sim dr^3 + er^\alpha$, $\alpha > 3$ being the spectrum slope, and a, b, d, e some constants. From these results, it is easy to extract the exponents of the SD moments, i.e., $z_2^A = \alpha - 1$ and $z_3^A = \alpha$. For instance, in the case of run B, these would be $z_2^A = 2.4$ and $z_3^A = 3.4$. Actually, our data give the following values: $z_2 = 2.52 \pm 0.20$ and 3.62 ± 0.20, which are, however, compatible with the error bars on the estimated scaling exponents. For a comparison, we report in Fig. 9 the SD structure functions of order $p = 2,3$ with the predicted slopes of Ref. 30. The other runs give compatible results.

V. TEMPORAL STATISTICS

As is well known, in 3-D turbulence we can recast the temporal behavior of the velocity field into the spatial domain via the Taylor hypothesis (frozen turbulence hypothesis): the effect of large scales is just that of a uniform sweeping, which does not modify the small-scale structures

Downloaded 01 Oct 2011 to 130.89.86.11. Redistribution subject to AIP license or copyright; see http://pof.aip.org/about/rights_and_permissions

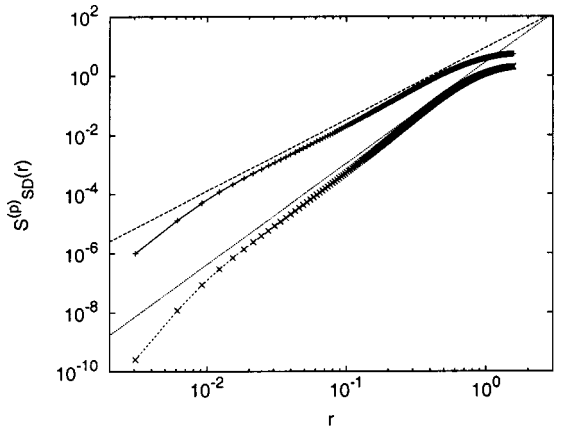

FIG. 9. A log–log plot of the SD structure functions of order $p=2$ (top) and $p=3$ (low), respectively. The continuous line scale with the exponents $z_2^A=\alpha-1$ and $z_3^A=\alpha$.

and their energy content. In two dimensions, the absence of a time hierarchy rules out such a possibility.[3,4,23] This is also evident by looking at snapshots from numerical simulations, which show that the time evolution of the dynamics is dominated by long-living structures (see Fig. 1). For such a reason it is nontrivial to predict the velocity temporal statistics collected in a fixed spatial location.

We performed a DNS of (2) with a large-scale, time-dependent forcing F, of constant amplitude at wave numbers $4<k_f\leqslant 6$. We performed a long time integration of the 2-D N–S equations, at resolution 512^2 and collected statistics for hundreds large eddy-turnover times, estimated as $t_{\text{eddy}}\approx 1/\omega_{\text{rms}}$ (for details on the numerical simulation see the note in Ref. 31). After the system reached a stationary state, we collected the time evolution of the velocity fields at some specific spatial locations with a sampling time $\tau_{\text{samp}}\approx 2.5\times 10^{-3}t_{\text{eddy}}$. Some observations are noteworthy. The first one concerns the *ergodicity* of the velocity field $\mathbf{u}(\mathbf{x},t)$. Temporal signals at different spatial locations possess different probability distribution functions. In particular, the range of variations of the local rms values $u_{\text{rms}}(\mathbf{x}_0,t)$ is so wide that we cannot average time histories recorded at different points. It is difficult to say if waiting long enough one would recover, as expected, some stable ergodic properties. With our statistics it is safe to report results only on local averages.

In particular, we chose two typical spatial situations: one, p_{in}, of a probe situated in the core of a vortical structure; the other, p_{out}, of a probe situated in a laminar region. This means that notwithstanding the turbulent evolution of the field, the motion of the vortices is so slow that probes almost maintain their respective ''character'' (*in* and *out* of a vortex) all the simulation long.

The time series recorded by the two probes display very different behaviors [see Fig. 10(a)]. To have a better understanding, it is useful to consider the frequency spectra $E(\overline{\omega})$ of the signals, calculated from the temporal Fourier transform of the stationary time correlation function, e.g., of $C[u_x(p),\tau]=\langle u_x(p,t+\tau)u_x(p,t)\rangle$.

In Fig. 10(b), we can observe the spectra of the two probes. At variance from the spatial spectra, it is not possible

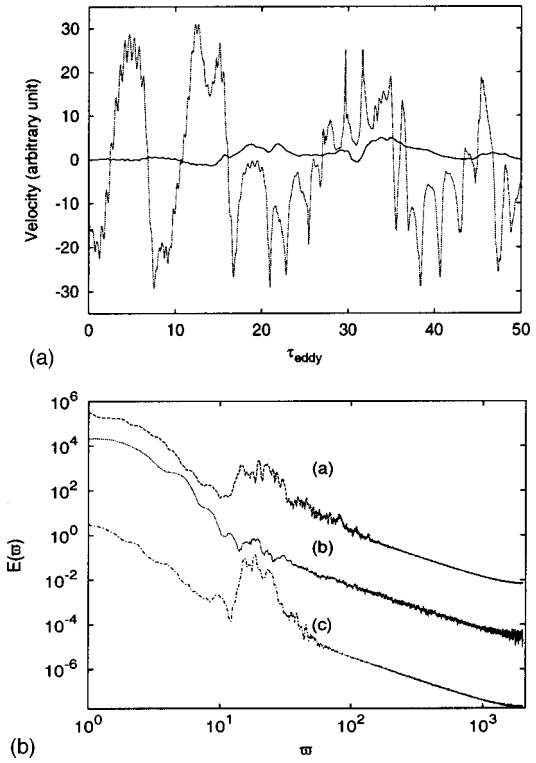

FIG. 10. (a) A time record of the x component of the velocity field of the p_{in} probe (dotted line) and the p_{out} probe (solid line); (b) a log–log plot of the frequency spectra of the following signals: (a) $E_{p\text{in}}(\overline{\omega})$ of the probe near a coherent structure; (b) $E_{p\text{out}}(\overline{\omega})$ of the laminar one; (c) $E_{k_f}(\overline{\omega})$ of the time evolution at a particular Fourier mode $\mathbf{k}$, in forced wave-number band $|k_f|=(4;6]$.

to extract a clear scaling behavior. One can only identify an exponential decay, and a peak region located at the frequency $\overline{\omega}^{(L)}\approx 0.51/t_{\text{eddy}}$ [here and in the sequel ''(L)'' stands for ''large scale'']. It is easy to recognize that $T^{(L)}$, defined as $T^{(L)}\equiv 1/\overline{\omega}^{(L)}$, is the typical time scale associated to the large-scale structures, either estimating it from the vorticity content of the largest structures $T^{(L)}\approx 1\sqrt{\langle\omega^2\rangle}$ or from their typical revolution time. In other words, Fig. 10(b) tells us that in each spatial point the time evolution is governed by the typical oscillation frequency of the forced large-scale structures. This is confirmed by the comparison of the probes' spectra with that built from the time correlation of the Fourier transformed velocity field $\hat{\mathbf{u}}(\mathbf{k},t)$ at a given mode $\mathbf{k}$, belonging to the forced wave number band. Indeed, all spectra poses a peak frequency $\overline{\omega}^{(L)}$.

Let us now investigate direct and inverse statistics of $\mathbf{u}(t)$. Direct structure functions behave trivially for both probes, $S_p(\tau)=\langle[u(\mathbf{x_0},t+\tau)-u(\mathbf{x_0},t)]^p\sim c_p\tau^p$, where u can be either one of the components (u_x,u_y) or the velocity modulus.

Since inverse moments do not possess good scaling laws, we refrain from giving any quantitative statement, while we concentrate on some qualitative properties showed by PDF's of temporal inverse events measured at the two probes, p_{in} and p_{out}.

In Fig. 11, for the probe p_{in}, we plot various PDFs $P[\tau_{\delta u}/\langle\tau(\delta u)\rangle]$, at varying δu, all rescaled with their mean

Downloaded 01 Oct 2011 to 130.89.86.11. Redistribution subject to AIP license or copyright; see http://pof.aip.org/about/rights_and_permissions

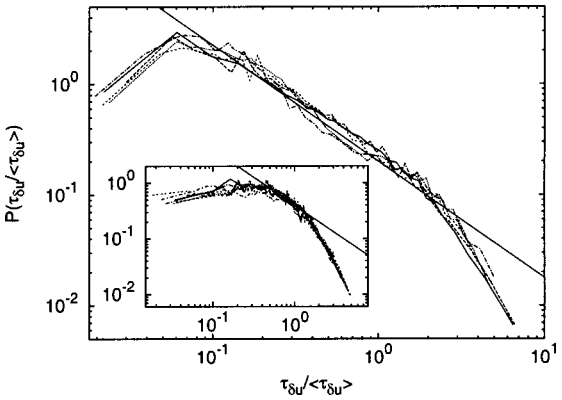

FIG. 11. Exit-time probability density functions $P(\tau_{\delta u})$ measured on the statistics of the probe p_{in}. The curves, calculated for different exit barriers δu, are normalized by their first moment. In the inset, the same for the probe p_{out}. In each figure, the straight line is the power law behavior $\tau_{\delta u}^{-1}$.

value $\langle \tau(\delta u) \rangle$. First we notice that PDFs collapse very well, indicating the absence of intermittency. Second, between the peak and the exponential tails at large τ, each probability density function exhibits, on a wide range of scales, a power law behavior $P(\tau_{\delta u}) \sim (\tau_{\delta u})^{-\gamma}$ with an estimated exponent $\gamma \approx -1$. On the other hand, PDFs measured on the probe outside the vortex, p_{out}, show a different behavior (the inset of Fig. 11). In particular, there is not any clear power law behavior. This indicates that very large exit events become less and less probable outside the vortex; we interpret this as the absence of very smooth fluctuations in the vortex background.

Although qualitative, the inverse statistics properties allow us to characterize the different temporal statistical behaviors associated to different fluid regions.

VI. CONCLUSION

To summarize, we studied inverse statistics moments for signals with a more than smooth spectrum, i.e., signals that are differentiable, and with nontrivial stochastic subleading fluctuations. We have shown that statistical velocity properties of 2-D turbulent flows are not simply described in terms of the spectrum slope. From the exit-distance analysis, it is possible to highlight a whole spectrum of smoother-than-differentiable fluctuations. These, being connected with laminar events, are the strongest statistical signature of the large-scale coherence. Experiments with different methods of removing/pumping energy at large scales should be performed, to investigated the importance of large-scale structures in the inverse statistics of flows with different spectra. We have quantified laminar fluctuations also by using second-order differences, i.e., direct velocity increments subtracted of their differentiable behavior. We have found also in this case that more-than-differentiable fluctuations are not simply described by one single exponent.

As a final remark, we stress that inverse statistics provide a completely new statistical indicator with respect to the standard direct statistics observables. We have shown that such method is necessary in all those cases where nontrivial fluctuations are subleading with respect to the differentiable contributions. Obviously, the same kind of analysis reported here can be extended to other temporal signals, applying the method to a broad class of natural phenomena. As an example, we just mention possible applications in situations common to climatology or meteorology, where estimating the probability of persistent velocity configurations, or of any other dynamical variable, is relevant. As a perspective, an important generalization is the investigation of multidimensional signals by studying the statistics of D-dimensional volumes between equispaced isosurfaces.

ACKNOWLEDGMENTS

We thank A. Vulpiani for his contribution to the early stage of this work. We acknowledge useful discussions with R. Benzi, G. Boffetta, and G. Eyink. This work has been partially supported by the EU under Grant No. HPRN-CT 2000-00162 ''Non ideal turbulence'' and Grant No. ERB FMR XCT No. 98-0175, ''Intermittency in turbulent systems.'' M.C. has been partially supported by the European Network ''Non ideal turbulence'' (Contract No. HPRN-CT-2000-00162). We also acknowledge INFM support (Iniziativa di Calcolo Parallelo).

[1] U. Frisch, *Turbulence: The Legacy of A. N. Kolmogorov* (Cambridge University Press, Cambridge, 1995).
[2] A. Celani, A. Lanotte, A. Mazzino, and M. Vergassola, ''Fronts in passive scalar turbulence,'' Phys. Fluids **13**, 1768 (2001).
[3] R. H. Kraichnan, ''Inertial range in two-dimensional turbulence,'' Phys. Fluids **10**, 1417 (1967).
[4] R. H. Kraichnan and D. Montgomery, ''Two-dimensional turbulence,'' Rep. Prog. Phys. **43**, 35 (1980).
[5] L. Smith and V. Yakhot, ''Bose condensation and small-scale structure generation in a random force driven 2D turbulence,'' Phys. Rev. Lett. **71**, 352 (1993).
[6] J. Paret and P. Tabeling, ''Intermittency in the two-dimensional inverse cascade of energy: Experimental observations,'' Phys. Fluids **10**, 3126 (1998).
[7] G. Boffetta, A. Celani, and M. Vergassola, ''Inverse cascade in two-dimensional turbulence: Deviations from Gaussianity,'' Phys. Rev. E **61**, R29 (2000).
[8] P. Santangelo, R. Benzi, and B. Legras, ''The generation of vortices in high-resolution, two-dimensional decaying turbulence and the influence of initial conditions on the breaking of self-similarity,'' Phys. Fluids A **1**, 1027 (1989).
[9] K. Nam, T. M. Antonsen, Jr., P. N. Guzdar, and E. Ott, ''k spectrum of finite lifetimes passive scalars in Lagrangian chaotic fluid flows,'' Phys. Rev. Lett. **83**, 3426 (1999).
[10] K. Nam, E. Ott, T. M. Antonsen, Jr., and P. N. Guzdar, ''Lagrangian chaos and the effect of drag on the enstrophy cascade in two-dimensional turbulence,'' Phys. Rev. Lett. **84**, 5134 (2000).
[11] K. Ohkitani, ''Wave number space dynamics of enstrophy cascade in a forced two-dimensional turbulence,'' Phys. Fluids A **3**, 1598 (1991).
[12] G. Boffetta, A. Celani, S. Musacchio, and M. Vergassola, ''Intermittency in two-dimensional Eckman–Navier–Stokes turbulence,'' Phys. Rev. E **66**, 026304 (2002).
[13] G. Falkovich, K. Gawçedzki, and M. Vergassola, ''Particles and fields in fluid turbulence,'' Rev. Mod. Phys. **73**, 913 (2001).
[14] M. H. Jensen, ''Multiscaling and structure functions in turbulence: An alternative approach,'' Phys. Rev. Lett. **83**, 76 (1999).
[15] L. Biferale, M. Cencini, D. Vergni, and A. Vulpiani, ''Exit time of turbulent signals: A way to detect the intermediate dissipative range,'' Phys. Rev. E **60**, R6295 (1999).
[16] M. Abel, L. Biferale, M. Cencini, M. Falcioni, D. Vergni, and A. Vulpiani, ''Exit-time approach to ϵ-entropy,'' Phys. Rev. Lett. **84**, 6002 (2000).
[17] M. Abel, L. Biferale, M. Cencini, M. Falcioni, D. Vergni, and A. Vulpiani, ''Exit-time and ϵ-entropy for dynamical systems, stochastic processes, and turbulence,'' Physica D **147**, 12 (2000).

Downloaded 01 Oct 2011 to 130.89.86.11. Redistribution subject to AIP license or copyright; see http://pof.aip.org/about/rights_and_permissions

[18]L. Biferale, M. Cencini, A. Lanotte, D. Vergni, and A. Vulpiani, ''Inverse statistics of smooth signals: The case of two dimensional turbulence,'' Phys. Rev. Lett. **87**, 124501 (2001).
[19]G. L. Eyink, ''Exact results on stationary turbulence in 2D: Consequences of vorticity conservation,'' Physica D **91**, 97 (1996).
[20]R. Salmon, *Geophysical Fluid Dynamics* (Oxford University Press, New York, 1998).
[21]M. Rivera and X. L. Wu, ''External dissipation in driven two-dimensional turbulence,'' Phys. Rev. Lett. **85**, 976 (2000).
[22]J. Paret, M.-C. Jullien, and P. Tabeling, ''Vorticity statistics in the two-dimensional enstrophy cascade,'' Phys. Rev. Lett. **83**, 3418 (1999).
[23]V. Borue, ''Spectral exponents of enstrophy cascade in stationary two-dimensional homogeneous turbulence,'' Phys. Rev. Lett. **71**, 3967 (1993).
[24]C. V. Tran and T. G. Shepherd, ''Constraints on the spectral distribution of energy and enstrophy dissipation in forced two-dimensional turbulence,'' Physica D **165**, 199 (2002).
[25]It can be shown that moments calculated in this way are the same as those calculated from a sequential average, i.e., ''scanning'' consecutively the time series and then using a suitable renormalization; see Ref. 15 for details.
[26]G. Parisi and U. Frish, ''On the singularity structure of fully developed turbulence,'' in *Turbulence and Predictability in Geophysical Flows*, Proceedings of the International School of Physics ''E. Fermi,'' edited by M. Gail, G. Parisi, and R. Benzi (1985).
[27]J. O'Neil and C. Meneveau, ''Spatial correlations in turbulence: Predictions from the multifractal formalism and comparison with experiments,'' Phys. Fluids A **5**, 158 (1993).
[28]R. Benzi, L. Biferale, and E. Trovatore, ''Ultrametric structure of multiscale energy correlations in turbulent models,'' Phys. Rev. Lett. **79**, 1670 (1997).
[29]R. Benzi, S. Ciliberto, R. Tripiccione, C. Baudet, F. Massaioli, and S. Succi, ''Extended self-similarity in turbulent flows,'' Phys. Rev. E **48**, R29 (1993).
[30]D. Bernard, ''Influence of friction on the direct cascade of the 2nd forced turbulence,'' Europhys. Lett. **50**, 333 (2000).
[31]In this series of numerical simulations, enstrophy is dissipated by a hyperviscosity term with $q=4$, while energy is removed using an IR drag term with $\rho=2$. The resulting (spatial) energy spectrum has the form $E(k) \sim k^{-\alpha}$, with $\alpha=5.0\pm02$.

Downloaded 01 Oct 2011 to 130.89.86.11. Redistribution subject to AIP license or copyright; see http://pof.aip.org/about/rights_and_permissions